Biophysical Chemistry 139 (2009) 123–136

Contents lists available at ScienceDirect

Biophysical Chemistry

journal homepage: http://www.elsevier.com/locate/biophyschem

A LB film morphological study with reference to biopolymer–surfactant interaction taking gelatin–CTAB system as a model

Debolina Mitra, Subhas C. Bhattacharya, Satya P. Moulik *

Centre for Surface Science, Department of Chemistry, Jadavpur University, Kolkata-700 032, West Bengal, India

ARTICLE INFO

Article history:
Received 30 August 2008
Received in revised form 27 October 2008
Accepted 29 October 2008
Available online 9 November 2008

Keywords:
Gelatin–CTAB interaction
LB film
Adsorption isotherm
Kinetics
Topography by SEM, AFM and ellipsometry

ABSTRACT

The interaction of gelatin with cetyltrimethylammonium bromide (CTAB) studied at pH 9 and an ionic strength of 0.005, produces an interfacial surface active gelatin–CTAB (monomer) complex (GS^{I}_{n}), a surface inactive gelatin–CTAB (micelle) complex in bulk (GS^{B}_{m}), followed by coacervation, and its solubilization in micellar solution of CTAB. We have herein attempted to probe the interfacial morphological changes of gelatin and its CTAB complexes, and not the bulk properties like coacervation and/or micellar solubilization. The morphologies of pure gelatin and CTAB films and that of gelatin–CTAB interacted complex at the interface have been investigated using LB, SEM, AFM and ellipsometric techniques. The stability of the gelatin monolayer at varied concentrations with and without CTAB has been examined. The SEM images of stabilized films of gelatin and gelatin–CTAB complex have witnessed compact smooth as well as rough surfaces with formation of distinct domains. Drastic morphological change in the film before the critical aggregational concentration of CTAB (T_2) has been in line with an initial abrupt decrease in surface tension. This has been corroborated by AFM measurements, which along with morphology demonstration has provided information on the diameter of the ensembles formed and roughness of the LB films constituted of pure components and their complexes. Thickness of the film was at its maximum in the domain region, as corroborated by ellipsometric technique. Such an elaborate interfacial monolayer and film morphology study of biopolymer-amphiphile system has been rarely documented in literature.

1. Introduction

Proteins are complex macromolecules having different levels of structures. The interfacial adsorption dynamics of a protein depend on the positions of the amino acids in the chain, and its various hydrophobic side chain groups. The polar and ionic groups contribute to the hydrophilicity of the protein, whereas non polar groups contribute to its hydrophobicity. Once adsorbed on a surface, the protein may rearrange and unfold by thermodynamic forces and undergo denaturation at the interface. At the air/buffer interface, the protein by losing its nativity may spread and reduce the interfacial tension; it can rearrange in various time scales, and models have been developed to address this issue [1]. Recent studies have focused on enhancement of interfacial adsorption of protein by choosing appropriate adsorbing surfaces, optimizing protein structure by chemical and/or physical modifications, etc. The Langmuir–Blodgett (LB) technique (a two-dimensional model surface pressure-measuring device) is in the use to meet such requirements [2,3].

Extensive studies have appeared on Langmuir monolayer (LM) isotherms of polymer, polysaccharides, polyelectrolytes [4], amphiphiles like lipids, natural phospholipids, synthesized functional amphiphiles [5], geminis [6], dendrimers [7], peptide-phospholipid mixed monolayers [8], bovine/goat pulmonary lung surfactants [9,10] etc with attempts of modification of their morphologies either to enrich or subside adsorption. LB deposition of single monolayers of a surfactant to modify surface roughness has been also attempted [11].

Polyelectrolyte-surfactant complexation is a challenging topic for study. Previous studies on polyelectrolyte-surfactant complexes have focused mainly on their bulk properties and self-assembly; less work has been done to elucidate the role of interface in the growth and nucleation of these complexes. The principal technique that has been used is tensiometry, especially for weakly interacting systems [12]. The LM technique has been frequently used to study the interaction of substances dissolved in the aqueous subphase, e.g. ions, drugs, enzymes with the components of the monolayers formed at the interface. The shapes of the isotherm are indicative of the interactions among molecules in the monolayers, and between molecules of the monolayers and that in the subphase. Studies on the interaction of a polymer/protein with charged or zwitterionic surfactant/lipid through LM are both convenient and informative, but such studies are fewer in number since strongly interacting systems are difficult to characterize

* Corresponding author. Tel.: +91 33 2414 6411; fax: +91 33 2414 6266.
E-mail address: spmcss@yahoo.com (S.P. Moulik).

0301-4622/$ – see front matter © 2008 Elsevier B.V. All rights reserved.
doi:10.1016/j.bpc.2008.10.012

[13,14]. Interaction of an anionic polyelectrolyte with cationic CTAB at various stages of association has been assessed from tensiometric isotherms [15,16]. It has been found that for interaction of polyoxyethylene with bilayers of a non ionic surfactant, the head group area of the latter plays a controlling role [17].

In the past decade, methods like Brewster angle microscopy (BAM) [16], fluorescence microscopy [18], X-ray reflectivity [15], atomic force microscopy (AFM) [19], scanning electron microscopy (SEM) [13], X-ray diffraction and scattering [20], neutron reflectometry [21] and dynamic/static light scattering [22] have been employed to understand the interfacial density profile or out-of-plane LM transitions. Fluorescence microscope has been used to characterize the bile acid mixed plant/animal sterol monolayer with distinct domain formation depending on the mixing mole ratio [23]. SEM images have been considered to portray two dimensional morphology of the LM. AFM has been considered to be more reliable and it is the only existing method for a direct 3D visualization of polymer chains, protein monolayers [24], micellar shape variations with counterions etc [25], adsorption on oppositely/like charged mica [26], silica [26], graphite [27], titanium oxide [28], glass [29], etc. AFM elucidation of polymeric monolayer at the air/solution interface near the state of collapse has revealed a complex irreversible 3D topography [30]. Ellipsometry has been playing an important role in the estimation of the thickness and refractive index of adsorbed layers of non ionic polymer solutions [31,32]. But studies on the morphological changes produced during a protein–lipid/surfactant interaction have been a few [33].

The studies of interfacial monolayers of proteins and biopolymers are important for their biological relevance and applicability in developing biomolecular devices [13,33,34]. The present study focuses on the monolayer of the denatured biopolymer, gelatin in its random coil configuration, in which one-third of the chain comprises glycine (~33%) and ~22% contribution comes from either proline or hydroxyproline. The rest of the constituents are mainly basic group bearing amino acids like lysine and arginine (~7.5%), acidic group containing representatives like glutamic acid and aspartic acid (~12%) and also leucine, isoleucine, methionine and valine (~6%). The protein has an isoelectric pH (IEP) of 4.84. At the present studied pH of 9.0, gelatin was fairly negatively charged. This investigation essentially comprises the LM of pure gelatin at pH 9, the adsorption kinetics of the protein at the air/buffer interface, changes in its LM on interacting with CTAB in relation to tensiometric measurements. We have also studied the morphological changes in the interaction profile from SEM images. AFM images have provided additional information on the 3D topography and texture at the surface. Ellipsometric measurements have offered information on the relative thickness, refractive index and surface excess of the adsorbed gelatin–CTAB film. A comprehensive physicochemical account of the interfacial behavior of the biopolymer and its interacting complex with the oppositely charged amphiphile, CTAB viewed by different techniques has been presented in what follows. The results obtained, we believe, would serve as a model for the understanding of biopolymer-surfactant/lipid interaction at the air/buffer interface in relation to composition variation in the system.

2. Materials and methods

All measurements were taken in boric acid-borax buffer medium at pH 9, and at a very low ionic strength, μ=0.005. The biopolymer solution was prepared as reported earlier [35]. The concentrations of gelatin used were expressed in g% (w/v).

2.1. Materials

Gelatin (weight average molar mass of 38,000 g mol^{-1}, and IEP=4.84) was a product of Sigma (USA), the sample we used earlier [35–37]. CTAB and chloroform were AR and HPLC grade products of Aldrich (USA). Borax and boric acid were AR grade products of Merck (India). The purity of all the samples used was >99%, since surface-active impurity makes appreciable changes in the monolayer property [3]. The water used in the study was doubly distilled conductivity water of specific conductance 2–4 μS cm^{-1} at 303 K. CTAB produced the expected critical micelle concentration (cmc) as reported in literature [35], and no minimum in the γ (surface tension) vs log [surfactant] plot was observed (Fig. 1) [35]. Thus, the material was free from any surface active species other than CTAB.

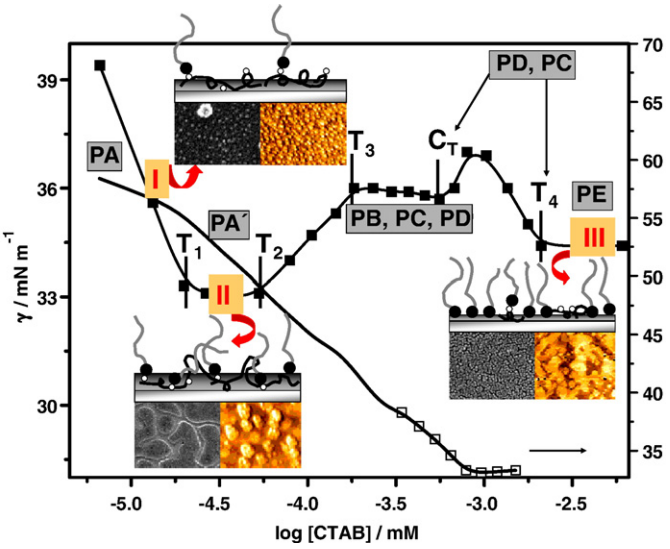

Fig. 1. Schematic diagram of the tensiometric profile (γ vs. log [CTAB]) for pure CTAB in buffer (open symbols), and in presence of 0.2 g% gelatin (with solid symbols) at 303 K. For pure CTAB, symbols for the initial stage are not shown to reduce clumsiness. The stages I, II and III denote CTAB concentrations at pre T_1 [0.013 mM], pre T_2 (cac) [0.033 mM] and post T_4 (cmc_2) [3.06 mM] conditions at which LB, AFM, SEM and ellipsometric measurements were taken. In the corresponding revealing depictions, the upper section is a conceptual projection of the interface (dark shaded), the subphase (light shaded) and the experimentally found SEM (LHS) and AFM (RHS) images (bottom section).

2.2. Methods

2.2.1. Tensiometry

Tensiometric measurements were taken with a calibrated du Nouy tensiometer (Kruss, Germany) by the ring detachment technique. 10 mL gelatin solution of desired concentration in aqueous buffer solution was taken in a thermostated (accuracy within ±0.1 K) double walled (for circulating temperature controlled water through the annular space between the walls) glass container at 303 K. A stock CTAB aqueous solution of desired concentration (~10–16 times cmc) was stepwise added in it with a Hamilton microsyringe, stirred well using magnetic stirrer at each addition, and 20 min equilibration time was allowed prior to taking measurements. The detailed procedure for γ measurements has been reported earlier [35]. The experiments were duplicated to check reproducibility. The γ values were accurate within ±0.1 mN m^{-1}.

The relative Gibbs surface excess of the saturated CTAB monolayer at the air/solution interface (Γ^{T}_{max}) was calculated from the slope of the linear profile of tensiometric isotherm up to cmc from the relation [35],

$$\Gamma^{T}_{max} = -1/(2.303nRT) \underset{[CTAB]\sim cmc}{Limit} d\gamma/d\log[CTAB] \quad (1)$$

where n, R, T and [CTAB] are the number of species formed per surfactant monomer in solution (which was 2 for CTAB by ionization),

the universal gas constant, absolute temperature and the molar concentration of CTAB in solution, respectively.

2.2.2. Langmuir film balance

A Langmuir balance of Apex Instrument Co. (India), Model LB2000C with vibration isolation was used for surface pressure–area isotherms. The trough and the barrier were made up of Teflon (both hydrophobic and lipophobic) to avoid contamination from the subphase. A Plexiglas box to prevent entry of dust particles covered the stage and trough. The subphase was either buffered gelatin solution (at the desired concentration) or aqueous buffer solution. Wilhelmy plate method using a filter paper strip (Whatman 2, ~1.7×0.8 mm^2 peripheries), having a zero contact angle with the buffer subphase and no free rotation was employed. Initially, the filter paper strip was allowed to completely wet by the subphase. The changes in surface pressure (π) were measured using a film electrobalance (Sartorius), connected to a computer. The surface pressure balance had a resolution of 0.01 mN m^{-1}. The surface of the buffer subphase was cleaned using a micropipette aspirator. All measurements were taken at a subphase temperature of 299±0.5 K at a lateral compression rate of 5 mm min^{-1}. Duplicate runs were taken to check reproducibility.

2.2.2.1. Preparation of Gibbs monolayer of gelatin. A requisite volume of gelatin in buffer solution from a stock concentration of 0.05 mg/mL was added on the top of the buffer subphase and was softly agitated for a while to assist spreading before inserting the filter paper strip in the subphase. The system was then allowed time for spreading and equilibration. A steady increase in π for a short period (~15 min) was observed before attaining equilibrium; this has also been reported earlier [38]. The equilibrium value did not change if longer time period was allowed.

For the detection of surface pressure–area (π–A) isotherm, compression was started after 15 min. For tracing the monolayer stability feature, it was compressed up to π=14 mN m^{-1} and the change in π was traced against time.

2.2.2.2. Preparation of gelatin–CTAB Langmuir monolayer. CTAB solution in chloroform at a concentration of ~20 mg/mL was smoothly delivered on the top of buffered solution of gelatin (0.2 or 0.05 g%) as the subphase with a Hamilton microsyringe. It spread on the subphase. The solvent was then allowed to evaporate out to form the gelatin interacted CTAB monolayer.

For studying the kinetics of interaction, the change in π was traced against time without compressing the monolayer. For the measurement of π–A isotherm, an initial equilibration time of 50 min was required for the system to reach the equilibrium state.

2.2.2.3. Film preparation for AFM/SEM/ellipsometric measurements. The surface morphology of the LB film was studied using SEM and tapping mode AFM techniques, at a constant π of 10 mN m^{-1} (for pure gelatin) and 30 mN m^{-1} (in presence of CTAB). Measurements were taken at three CTAB concentrations: pre T_1 or stage I at [CTAB]=0.013, pre T_2 or stage II at [CTAB]=0.033, and post T_4 or stage III at [CTAB]=3.06 mM (Fig. 1). Constant surface tension is, however, not a reliable criterion for the thermodynamic equilibrium for polyelectrolyte/surfactant solutions. The adsorbed amount of both polyelectrolyte and/or surfactant composition at the surface layer as well as the surface structure can change, although π remains almost constant [39]. Keeping in mind that changes of the mean thickness at the initial stage of observation may lead to an inadvertent error in the concentration range under investigation, the time span for deposition was extended to ensure an equilibrium condition of the monolayer. Deposition procedures were initiated after an equilibration time of 1 hr to keep the morphology of the deposit unaltered during the operation.

CTAB solutions did not wet glass well due to the formation of a hydrophobic monolayer on the glass surface [40]; silanized silicon substrate was, therefore, used [41–43]. The silicon oxide surface was silanized with dichlorodimethylsilane, according to the recommended procedure [44,45]. The substrate provided good optical properties for adsorption studies (highly reflecting). It was found flat and featureless with low surface roughness (AFM on deconvolution of image indicated a roughness of less than 0.5 nm) and a maximum height variation of 0.10 nm across a 200 nm scan range [46–48]. Vertical dipping technique was used for deposition, and the substrate lift out rate from the subphase was 1 mm/min. The film was dried in air and examined.

2.2.3. SEM imaging

The surface morphology of the film was studied by high resolution field emission scanning electron microscope (FE SEM, Model No. JEOL JSM-6700F, Japan). The film was gold plated for 1 min under 5.5 mA current at an ambient temperature of 299±1 K.

2.2.4. AFM imaging

Topographic and phase images of the surface were taken in a DICP2, Veeco, USA (Model No. AP 0100) atomic force microscope. The protein was imaged in its natural buffer environment. To minimize any force exerted on the protein from the scanning tip, the AFM was operated in tapping mode in air. Thin phosphorus doped silicon cantilever (with no coating on the front side and a 50±10 nm aluminium coating at the back) of resistance 1–10 Ω cm was used for scanning. The thickness of the cantilever ranged from 3.5 to 4.5 μm with a length of 115–135 μm and width of 30–40 μm. With a nominal spring constant of 0.10 N m^{-1}, it was oscillated with a resonance frequency of 300 kHz at a scanning frequency of 0.5–1.0 Hz. The radius of curvature of the etched silicon tip used was 10 nm.

The deposited silicon substrate was dried in air at room temperature. Measurements were taken in air at an ambient temperature of 299±1 K and relative humidity of 92%.

2.2.4.1. AFM image analysis. The artifacts that can arise from the AFM tip area was taken care of by deconvolution of the AFM images using Veeco di SPM Lab NT version 6.0.2. The processed images were thereafter analyzed for diameter, height and surface roughness of the moieties by Proscan 1.8 Image analysis 2.1. The vertical bar corresponding to the height profile (Z-axis) is depicted in the left hand side bar for each AFM image. All images were flattened with a first order algorithm to correct for piezo-derived differences between the scan lines. R_{rms} represents the root-mean-square surface roughness, $\overline{H}$ denotes the mean height in the selected profile, and R_{p-v} gives the distance between the highest peak and lowest valley within a selected profile. Since the proteins appeared mostly round in the X–Y plane, 2-D profiles in the X–Z plane were drawn on the images as a diameter line passing through the centre. The distance between the two extremities of the line that was delimiting the feature was the diameter, and the height was the Z-value observed in the centre of the circle delimited by the diameter (cf. Fig. 6C). Repeat experiments produced images similar to that herein presented.

2.2.5. Ellipsometry

The ellipsometric measurements were performed with Gaertner Autogain L116B equipment of Gaertner Scientific Corporation (USA). The angle of incidence of the monochromatic beam (~1 mm diameter) of wavelength λ=632.8 nm (He–Ne laser) was 45°. Two independent angles were obtained applying Fresnel's equation that depends on the properties of the reflecting surface: the azimuth (Ψ) is the amplitude ratio for the reflected components parallel and normal to the plane of incidence, and Δ is the phase difference between them. To obtain the mean refractive index (n_x, in the bulk direction normal to the air/buffer interface) and the thickness (δ_x) of the adsorbed layer from the

measured ellipsometric angles Δ, Ψ, Δ_0 and Ψ_0 (the latter two characterize the bare air/buffer or gelatin-air interface), a numerical iteration procedure with a modified version of two angle LGEMP program was used. In the calculation, the following assumptions were made: (1) the film was non absorbing (~90% transmittance was observed in spectrophotometer (Shimadzu 1601 UV–VIS spectrophotometer) at 632.8 nm; (2) the experimental errors in the values of Ψ and Δ were less than 0.02 and 0.01°, respectively (this led to ~5% errors in the layer thickness and refractive index); (3) the refractive index of the environment corresponding to air was regarded as unity and that of buffer subphase was taken to be ~1.34; (4) the adsorbed layer was considered to be relatively thick and it was assumed that the refractive index of the adsorbed layer was related to the [protein]. Under these assumptions, the adsorbed amount Γ^{E}_{max} was calculated using the de Feijter equation [49,50],

$$\Gamma^{E}_{max} = \frac{\delta_x(n_x - n_s)}{dn/dc} \quad (2)$$

where n_s is the refractive index of the solvent and dn/dc is the refractive index increment in the system under investigation. For the gelatin–CTAB complex, dn/dc was taken to be 0.17, which was close to that of gelatin (0.19) and CTAB (0.15) [51,52]. For pure gelatin or CTAB or gelatin–CTAB complex, the deposition procedure on silicon wafer (refractive index of substrate n_0=3.85) followed was as detailed previously. With reference to Fig. 1 discussed below, depositions were taken at the indicated concentrations corresponding to stages I (gelatin–CTAB monomeric complex), II (gelatin–CTAB micellar complex, before precipitation) to obviate polarized or depolarized scattering of the laser beam in turbid solution with non homogenous interface, and at III (post precipitation, clear and feebly scattering stage). It was assumed that the adsorbed phase was homogenous and isotropic.

Ellipsometry gives a rather complex average of the film thickness [53]; contributions from different regions of the surface layer influence the mean value. Consideration of a large number of experimental points allowed the determination of the mean thickness with reasonable accuracy. The relative errors in the adsorption values were much less than the errors in n_x and δ_x. The errors became mutually compensated during the calculation of the adsorbed amount [53].

3. Results and discussion

3.1. γ-log[CTAB] isotherm

Typical tensiometric plots for pure CTAB, and CTAB in presence of 0.2 g% gelatin are illustrated in Fig. 1. A detailed description of the isotherms has been described in a previous report [35]. A brief synopsis is herein presented. Gelatin is a surface active denatured protein and settles preferably at the air/buffer interface (G^I) at equilibrium. On CTAB addition, three different stages has been marked as stages I, II and III, the former two being interfacial complexation, and the latter portraying both interface and bulk features. A schematic representation of the interface is profiled in the depiction of Fig. 1. The stage I represented the formation of gelatin-monomeric CTAB complex (GS^I_n) that preferably resided at the interface being more surface active than G^I. The following equilibrium arose till T_1,

$$G^I + nS \rightarrow GS^I_n \quad \text{(Process A or PA)}$$

An initial interfacial complexation was also evidenced from a significant reduction of γ from 56.2 for pure 0.2 g% gelatin to 39.4 mN m^{-1} with [CTAB]=0.007 mM.

GS^I_n was basically an ion pair between CTA^+ and negatively charged G^I at pH 9. Addition of more CTAB formed a plateau at stage II where it interacted with gelatin in the bulk (G^B) up to T_2 (critical aggregational concentration or cac), following the scheme,

$$G^B + nS \rightarrow GS^B_n \quad \text{(surface inactive complex)} \quad \text{(Process A′ or PA′)}$$

In this regime, tensiometry revealed no characteristic feature of the surface. It yielded a constant γ. At T_2, small CTAB aggregates associated with the biopolymer chain to form the "necklace-bead" type product GS^B_m in the bulk, with a consequent enhancement in γ in the T_2–T_3 range. Thus,

$$GS^I_n + CTAB(\text{aggregates}) \rightarrow GS^B_m \quad \text{(Process B or PB)}$$

Beyond T_3, two simultaneous processes were in operation along with the process B: replenishment of the bare interface with CTAB monomers occurred following the scheme,

$$I + x\text{CTAB} \rightarrow I(\text{CTAB})_x \quad \text{(Process C or PC)}$$

and a secondary process of aggregation and coacervation of the neutral interacted species, GS^C_m, following the equilibrium arose,

$$yGS^B_m \leftrightarrow \left(GS^B_m\right)_y \text{ or } GS^C_m \quad \text{(Process D or PD)}$$

The process ended at T_4 (extended cmc or cmc_2) with a gradual resolubilization of the interacted species in the micellar environment,

$$GS^C_m + \text{free CTAB micelle} \leftrightarrow GS_m(CTAB)_{MS}(\text{soluble}) + \text{free CTAB micelle}$$

(Process E or PE)

Further amphiphile dosing formed the plateau region at stage III with increasing concentration of free micelles in solution, forming complex, $GS_m(CTAB)_{MS}$. Probable information on the constituents of interface can be obtained by comparing γ of pure CTAB monolayer at the saturation level (33.2 mN m^{-1}) as against γ_{T4} of the interacted species at III (34.4 mN m^{-1}). The difference was ascribed to the combined occupancy of CTAB along with the less surface active free G^I and unreacted GS^I_n complex at the interface. In the subsequent sections, the result on the surface morphology and topography at the aforesaid stages I, II and III using LB, SEM, AFM and ellipsometric techniques, will be discussed.

3.2. Gibbs monolayer of gelatin and its stability

3.2.1. π–t isotherm to assess the stability

The monolayers of buffered gelatin (without compression) at concentrations 5 μg to 0.2 g% exhibited variable initial surface pressure (π^0_G) that stabilized after a short time (t^0_G) specific for each concentration. For a comparative study, the monolayers were compressed to a constant π=14.0 mN m^{-1}, and surface pressure–time (π–t) kinetics were followed. An initial steep rise in π up to a point called π^1_G within a time frame of t^1_G min was observed. The rise progressed with a decreased slope up to π^2_G; at t^2_G it attained a steady pressure, thereafter (Fig. 2A, main plot for 0.2 g%). The first step of the kinetic process was diffusion-controlled, like that of poly(dimethyldiallylammonium chloride) (PDMDAAC) [54]. Gelatin is a surface active protein, and it preferably diffused to the interface from the bulk to attain equilibrium. Higher [gelatin] required lesser time (t^1_G) to attain π^1_G due to increased gradient of chemical potential [55]. Afterwards, gelatin underwent aggregation and/or conformational change at the interface till reaching π^2_G. The combined phenomena required time for adjustment: higher [gelatin] required more time (t^2_G). A clear demarcation between π^1_G and π^2_G was not visible for the lowest [gelatin]=5 μg% (Fig. 2A, main

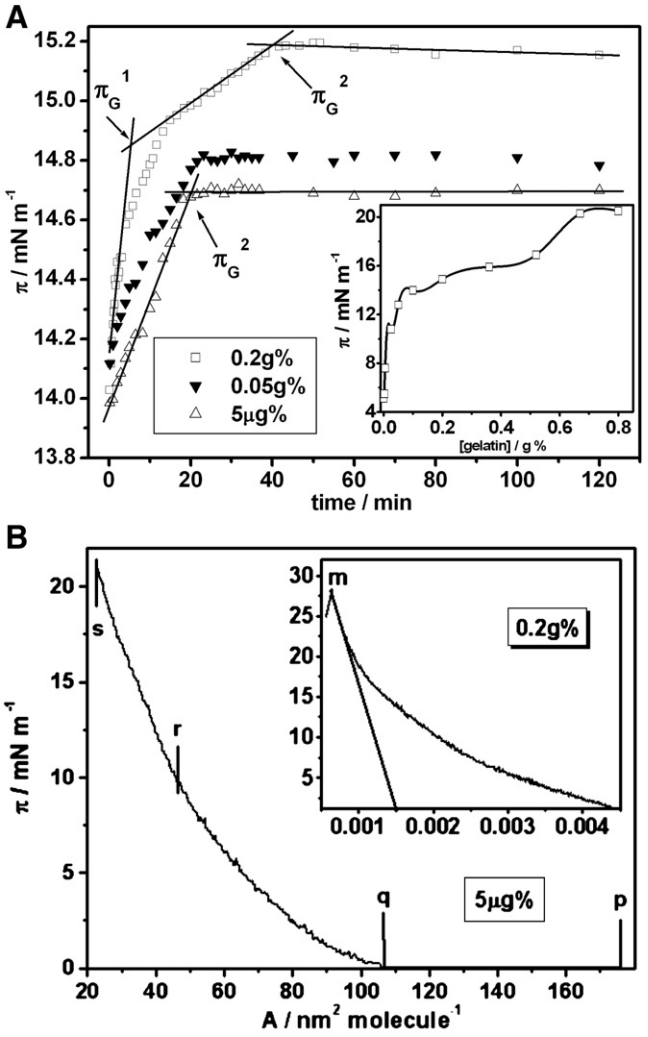

Fig. 2. π–t (in min) plot to study the kinetics of gelatin adsorption, and π–A isotherm of pure gelatin monolayer at 299 K. A. Main plot. π–t plot of compressed gelatin monolayer (at 14 mN m^{-1}) at varying [gelatin]= 5 μg, 0.05 g and 0.2 g%. Inset. π of uncompressed gelatin at varying [gelatin] by the ring detachment technique. B. Main plot. π–A isotherm for 5 μg% gelatin. Inset. Same for 0.2 g% gelatin. X- and Y-axis similar to that in the main plot.

plot). The comprehensive results are presented in Table 1a. The temperature and salt effects on the said phenomena would be interesting from the stand point of hydrophobic–hydrophilic behavior of the protein at the interface in relation to bulk. This was not under the purview of the present programme, and was left out for a future study.

3.2.2. π–A isotherm

The surface pressure vs area (π–A) isotherms were determined with varying [gelatin] also in the range of 5 μg–0.2 g%: results for the two extremities are presented in Fig. 2B. For the 5 μg%, initial surface pressure with a small value ran parallel to the X-axis, whereas for the second (0.2 g%), π started to rise from the beginning. With increasing [gelatin], increasing number of macromolecules resided at the air/solution interface: the systems were allowed some time (t_G^0) for their adjustment at the interface to reach the state of constant π called π_G^0 (Table 1a). Both t_G^0 and π_G^0 enhanced with [gelatin]. This was quite in contrast with lysozyme (0.05–1.3 mg%), in which an initial induction period was observed indicating a phase transition or conformational change allowing surface tension to remain constant over an extended period of time before the change was observed [56].

The 5 μg% gelatin isotherm produced the following features. Over a large advancement of the barrier position, π remained virtually zero (region p–q, main plot, Fig. 2B). At the exclusion area of 107 nm^2 $molecule^{-1}$, π started to rise, and increased non-linearly in the range between q and r. More compression made π to linearly increase (r–s) up to an upper limit of ~20 mN m^{-1} showing no tendency to collapse. For 0.2 g% gelatin, the initial flat region (observed for lowest concentration) was absent (Inset, Fig. 2B). A typical condensed type π–A isotherm appeared to steeply increase initially, without a liquid-expanded region. No distinct phase transition in the solid region was observed till the monolayer collapsed at π_c=28 mN m^{-1} (for 0.2 g% gelatin), a phenomenon similar to long chain alcohols, fatty acids and phospholipids [57]. Poly(N-isopropylacrylamide) (PNIPAM) monolayer isotherm has produced smaller π_c=30 mN m^{-1} like the herein studied gelatin [58]. Such a moderate collapse pressure (π_c) indicated that the LM was less compression friendly because hydrophobic interaction was counterbalanced by electrostatic repulsion between the negatively charged units in gelatin [4]. Collapse might start at a π as low as 25 mN m^{-1}, and depend exclusively on barrier speed as observed in monolayers of ytterbium biphthalocyanine or its derivatives [59,60]. Smaller surface pressure also indicated lesser amount of protein at the air/buffer interface. Thus, uncompressed gelatin solution of 0.2 g% produced π= 14.9 mN m^{-1} which increased to 20 mN m^{-1} at 0.8 g% (Inset, Fig. 2A) whereas the compressed layer in the LB method of 0.2 g% gelatin yielded a maximum π of 28 mN m^{-1}. The limiting areas of the isotherms (A_{min}^G), obtained by extrapolating the compressibility part of the curve to zero surface pressure, are given in Table 1a for varying [gelatin]. A decreasing trend with increasing [gelatin] was observed. Absence of a kink or plateau in the profile indicated that the transitions of the liquid-expanded, liquid condensed phases etc. were smooth. It may be pointed out that desorption of gelatin from the interface should affect the pattern of the isotherm. Since gelatin was fairly surface active (Inset, Fig. 2A) and the monolayer was slowly compressed (5 mm/min), after equilibration, the contribution of desorption was minimal.

3.3. Langmuir monolayer of gelatin–CTAB at stages I, II and III in the interaction profile

3.3.1. π–t isotherm and the kinetics

Addition of 0.013 mM CTAB to 0.2 g% gelatin at the interface induced cooperative electrostatic binding of gelatin resulting formation of interfacially active GS_n^I (via PA) which enhanced the effective hydrophobicity of the complexed protein. A marked increase in π from

Table 1
Surface pressure, time (t) taken to attain the said pressure and area minimum as observed in pH 9 buffer solution for (a), varying gelatin concentration, (b), 0.05 g% and 0.2 g% gelatin interacted CTAB system

(a)

[gelatin]/%	π/mN m^{-1}(t/min)			A_{min}^G [a]
	π_G^0 (t_G^0)	π_G^1 (t_G^1)	π_G^2 (t_G^2)	
5 μg	0.05 (5.4)	–	14.7 (20.1)	69.2
5 mg	1.05 (6.2)	14.4 (5.70)	14.8 (21.6)	0.077
0.05 g	1.25 (7.5)	14.6 (5.57)	15.0 (27.6)	0.006
0.2 g	1.45 (9.0)	14.8 (3.82)	15.2 (41.7)	0.001

(b)

[gelatin]/g%	[CTAB] [b]	π_{GC}^S (t_{GC}^S) [c]	A_{min}^S [a]	[CTAB] [b]	π_{GC}^S (t_{GC}^S) [c]	A_{min}^S [a]
	0.05			0.2		
Pre T_1 or stage I	0.013	23.4 (23)	12.2×10^{-3}	0.013	26.1 (34)	0.012
Pre T_2 or stage II	0.035	21.5 (20)	5.15×10^{-3}	0.033	24.1 (30)	4.7×10^{-3}
Post T_4 or stage III	1.622	20.2 (28)	7.71×10^{-5}	3.06	23.7 (40)	8.75×10^{-4}

[a] A_{min} (in nm^2 $molecule^{-1}$).
[b] [CTAB] in mM.
[c] $\pi_{GC}^S(t_{GC}^S)$ in mN m^{-1}(minutes).

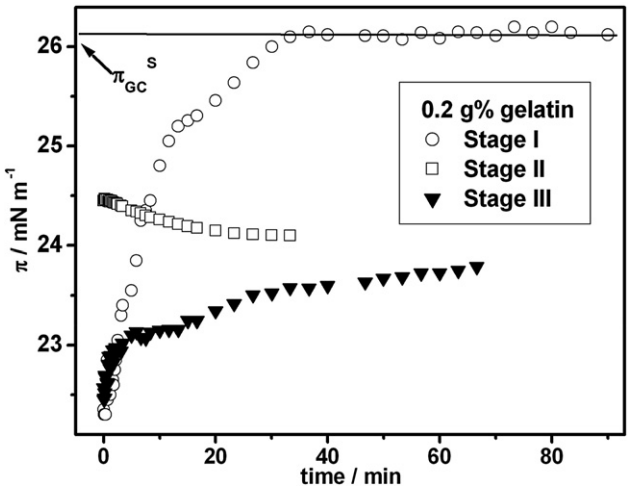

Fig. 3. π–t (in min) plot to study the kinetics of gelatin–CTAB interaction at 299 K.

1.45 mN m^{-1} (π_G^0 of 0.2 g% gelatin) to ~22 mN m^{-1} occurred after injection of the surfactant to the protein at the interface (Fig. 3). Injection of half of this [CTAB] to the monolayer made no significant difference, similar to earlier reports [4,38,61a]. This suggested an initial surface complexation, akin to strong oppositely charged polyelectrolyte-surfactant system. Thereafter, π attained a steady value of 26.1 mN m^{-1} (π_{GC}^{S}) in nearly 30 min (t_{GC}^{S}). The nature of the kinetic profile was similar to that of 0.2 g% gelatin in absence of CTAB (Fig. 2A, main plot). The surface pressure tended to decrease with time at stage II (Table 1b), suggesting either a rearrangement of molecules in the monolayer or partitioning of molecules into the subphase. In our earlier report [35], we have marked T_2 as the concentration at which GS_m^B started to form from GS_n^I following process B. Therefore, stage II marked the pre transition stage to surface inactive GS_m^B formation, that accounted for such a decrease in π_{GC}^{S}. Film morphological studies (illustrated later), have convincingly evidenced distinct morphological variation (domain formation) in this regime. Addition of 3.06 mM CTAB (stage III) resulted in a mild decrease in π: the trend was similar to the surface pressure at stage II and III (illustrated in Fig. 1). Similar profile was also observed for 0.05 g% gelatin. The kinetic course was on the whole comparable with stage I. The steady surface pressure values and the corresponding time are presented in Table 1b.

3.3.2. π–A isotherm with stabilized monolayer

The qualitative difference between the π–A isotherms of gelatin with and without CTAB was consistent with the formation of surface-active species, GS_n^I by the process A (PA). The slopes of the compressed isotherms became steeper with increasing [CTAB] but the levels of their rises consecutively declined (Fig. 4, main plot). A gradual transition from gaseous to liquid-expanded (LE) and then to liquid-condensed (LC) phase accounted for this observation, similar to the behaviors of monolayers of amphiphilic dendrimers [7]. With increase in [CTAB], a steep rise indicated a direct transition from 2-D gaseous phase to LC or solid phase. More GS_m^B complex was formed from GS_n^I (process PB) that dissolved in the bulk to decrease the interfacial concentration of both gelatin and CTAB to reduce the maximum value of π, along with its drastic decreased limiting area A_{min}^S (Table 1b). This critical area accounted for the contributions of surface active species. For 0.2 g% gelatin, A_{min}^S has the following trend. At stage I, it magnified ~10 folds than that of a pure gelatin monolayer. Gelatin–CTAB electrostatic complexation to GS_n^I was mainly limited to the local neutralization of free charges of the protein chain, occupying a reasonable area per molecule (Fig. 1, stage I). It then suffered reduction in two steps following two subsequent additions. The hydrophobic effect enhanced surfactant adsorption, and increased attraction of the protein segments among themselves as well as with the hydrocarbon tails of the surfactant at stage II. The adsorbed film contained small regions of low effective charge with high hydrophobic interaction between the components, thereby enhancing the compactness of the film with a simultaneous reduction in the limiting area (Fig. 1, stage II). The final stage III mainly referred to the limiting area of a pure CTAB monolayer, with an insignificant contribution of unreacted G^I or GS_n^I; as a result A_{min}^S decreased further (Fig. 1, stage III). As mentioned in Section 3.2.2, gelatin–CTAB surface layers particularly at higher [CTAB] were also prone to desorption. The process would be dependent on the rate of compression of the surface layer. Since we had used a fixed moderate compression rate of 5 mm/min and considered fair surface activity of the gelatin–CTAB complex, it minorly affected the results. To analyze the data in the light of a model such that of Fainerman et al. [61b] would not be meaningful until more experimental results were available under varied conditions.

3.4. SEM and AFM micrographs of gelatin, CTAB and their complex at stages I, II and III

To make topographical comparisons between the LB films of gelatin–CTAB and its parent components, SEM and AFM images at comparable component concentrations and magnifications have been taken. The SEM images portray dehydrated sample, whereas the AFM pictures represent hydrated samples at ambient condition. The deposition procedure as well as interaction of the adsorption layer with the solid support could induce structural changes in the film. Thus, comparison of the dimensions has been made on a relative basis than focusing on their absolute values. The results are presented in different sections below.

3.4.1. Pure CTAB

The interfacially adsorbed CTAB film transferred on silicon wafer surface at a concentration of 0.013 mM (<<cmc). The formed irregular structures in the SEM micrograph (Fig. 5A) were due to monomer aggregation during the sample drying process. But AFM images, scanning the molecules in the atomic level have evidenced topographical changes as depicted in Fig. 5B. Here the film contains mild artifacts. The cross sectional analysis has shown R_{p-v} of only 5.94 nm with a roughness of about 0.45 nm. The bearing plot (Fig. 5C) of the

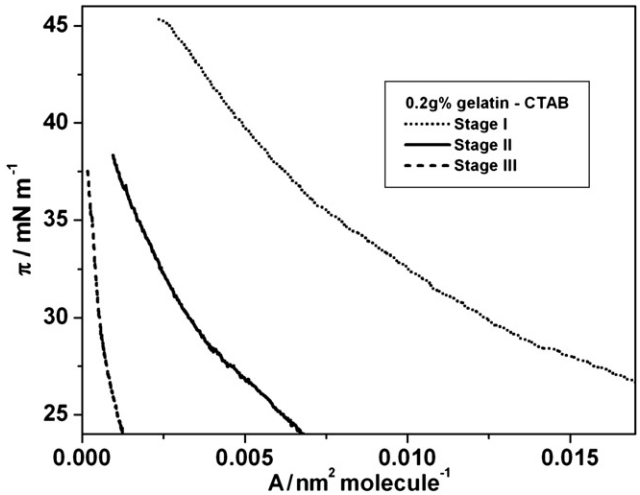

Fig. 4. π–A isotherm for 0.2 g% gelatin–CTAB interaction on adding CTAB at stages I, II and III (as illustrated in Fig. 1).

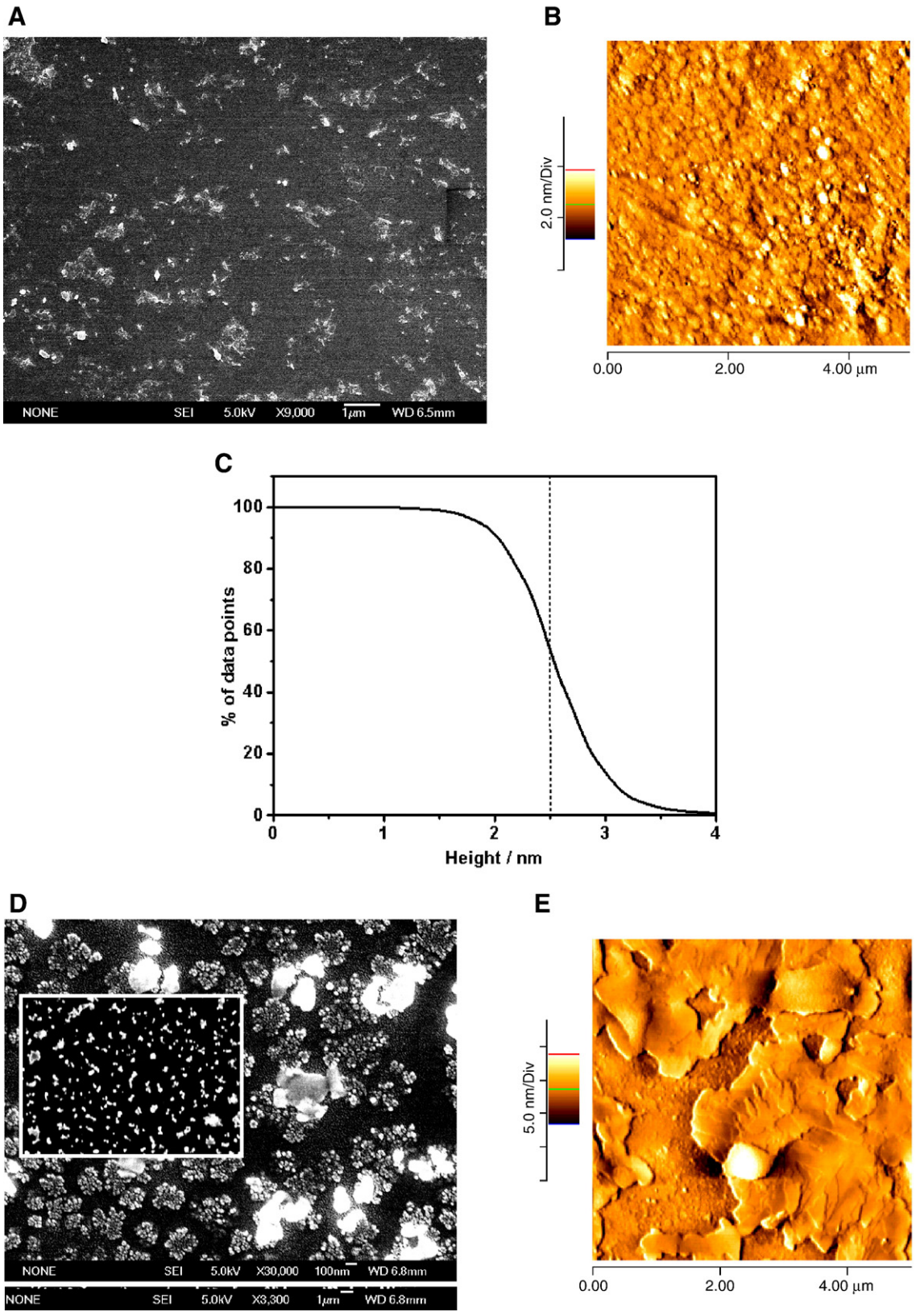

Fig. 5. SEM and AFM images of pure CTAB at concentrations corresponding to stages I and III (in Fig. 1). A, SEM image of pure CTAB at 0.013 mM (stage I). B, AFM image of the adsorbed films of pure CTAB film at stage I. C, Bearing plot of the region in Fig. 5B. Broken perpendicular line corresponds to the mean height of the region. D, SEM images of CTAB at 3.06 mM (stage III) at 30,000 magnification. Inset: At a 3300 magnification. Lower scale corresponds to that of the inset. E, AFM image of CTAB at 3.06 mM (stage III).

surface followed a steep fall within 2 to 3 nm, which suggested a jagged surface profile.

The images obtained by SEM at [CTAB] = 3.06 mM (~3 times cmc in the inset of Fig. 5D in lower magnification) showed homogeneity and continuity. The particles were uniformly distributed. Higher magnification evidenced the film consisted of discrete roughly circular spongy domains (Fig. 5D) with clustering at some places. The corresponding AFM representation (Fig. 5E) revealed flower petal

like domains, with a rough surface having rms value of 1.76 nm and $\overline{H}$ of 13.7 nm from the film surface. All the surface parameters (R_{rms}, $\overline{H}$ and R_{p-v}) enhanced with [CTAB]. For CTAB on silica at neutral pH, the adsorbate structure was reported to be either a bilayer (above cmc) [62] or hemispherical aggregates [63]. Manne et al. [64] observed hemimicelles (liquid crystalline aggregates) at the air/solution interface of a CTAB film adsorbate below cmc using contact mode AFM on graphite.

3.4.2. Pure gelatin at 0.2 g%

The SEM image of dried 0.2 g% gelatin film has evidenced patterned clusters of gelatin on silicon substrate (Inset, Fig. 6A) [27]. Gelatin is a good surface-active protein, and the activity enhanced with increasing [gelatin] (Inset, Fig. 2A). On zooming it on a smaller length scale (main profile, Fig. 6A), protein images as small aggregates of ~300 nm end-to-end distance were revealed. Presence of such clusters in a non-buffered environment ensured that they were not that of the salts. The surface protein images of gelatin in AFM in non contact mode have been illustrated in Fig. 6B. The diameter (D) and height (H) of a high profile protein cluster (Fig. 6C) were 133 and 0.40 nm respectively. In the figure, the contact mode image (Inset, Fig. 6B) was strikingly similar to the image of an AdhE protein of *E. coli* in phosphate buffer on a gold film (in contact mode AFM) or that of polystyrene-poly(methylmethacrylate) film at a lower magnification [65,66]. Large bare areas of a homogenous coating of protein film with protruding spherical/square islands (with a mean height of 6.31 nm) were visible. These images were stable and reproducible. Thus, upon adsorption at the air/buffer interface, solvated gelatin slowly diffused laterally to the surface, and aggregated in course of time in patches. The ability of a protein to get organized at the interface at low concentrations suggested interfacial assistance to the process [56]. Gelatin formed a smooth texture compared to pure CTAB film (at stage III); however, the surface roughness of CTAB image was minimum at stage I (Table 2). The obvious SEM and AFM image differences as in CTAB film was also observed for the gelatin film.

3.4.3. Gelatin–CTAB interaction

The interaction profile of gelatin–CTAB has been characterized at three stages: I (pre T_1), II (pre T_2) and III (post T_4) with reference to Fig. 1. On CTAB addition, the topography changed drastically and was quite different from the pure films. The features are described and discussed in the following subsections.

3.4.3.1. Pre T_1 or stage I. At [CTAB] = 0.013 mM, the SEM image domain of the water free sample appeared as uniform spotted distribution of small particles as a base with a random distribution of protruding globular islands of diameters 40 to 80 nm on it (Fig. 7A). This was taken as the initial formation of GS^{I}_{n}. The diameters of the high profile clusters were much reduced compared to that in pure gelatin (Fig. 6A). The AFM profile (Fig. 7B) has evidenced a uniform distribution of small nearly globular aggregates. In it, the high profile clustered bodies were, however, too few in number and too rough to image. CTAB addition to G gelatin film smoothened the surface roughness and reduced the mean height of the particles from 6.31 nm (in pure gelatin) to 2.10 nm (Fig. 7C) in presence of 0.013 mM CTAB. Here distinguishable globular aggregates appeared in comparison with a featureless topology of pure CTAB at this concentration (Fig. 5B).

3.4.3.2. Pre T_2 (cac) or stage II. Further addition of CTAB produced distinctive SEM images of interlinked bean shaped sponge-like domains with less than 0.5 μm voids (main representation, Fig. 8A). They were conspicuously separated from one another by thin bare areas in between as a consequence of repulsive interaction between the domains [16]. The increased number density of the surface

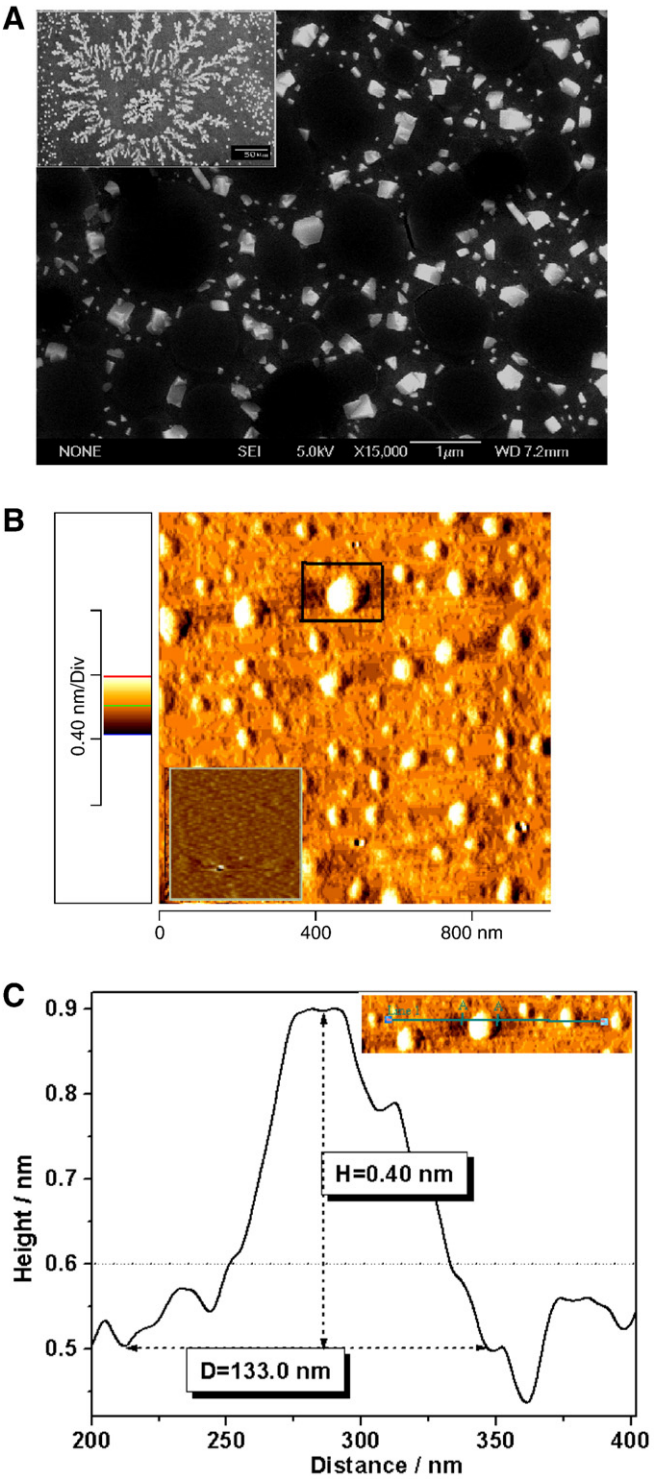

Fig. 6. SEM and AFM images of gelatin at 0.2 g%. A, SEM image at 15,000 magnification. Inset: Same image at 350 magnification. B, Non-contact mode AFM image of gelatin immobilized on silicon substrate. Inset: Same image in contact mode in a 10×10 μm frame size with the *Z*-axis ranging from 0–35 nm. C, height (*H*) and diameter (*D*) of high profile protein cluster as indicated by the segment AA′ in the inset of the figure. Broken perpendicular line represents mean height along line 1 in the inset. Inset: projection from the indicated box in Fig. 6B.

domains enhanced the layer thickness (as evidenced from ellipsometric studies discussed in the next section), and consequently caused expansion of the film. Buckingham et al. [67] pointed out that the complexation started at the interface having relatively higher concentration than the bulk; a 'gel' like adsorbed layer was formed

Table 2
The root mean square roughness (R_{rms}), mean height ($\overline{H}$), maximum peak to minimum valley distance (R_{p-v}), mean thickness (δ_x), mean refractive index (n_x) and surface excess of the adsorbed layer in a LB film[a]

	R_{rms}/ nm	$\overline{H}$/ nm	R_{p-v}/ nm	δ_x/nm	n_x	Γ^E_{max}/mg m^{-2}
0.2 g% gelatin–CTAB interacted combinations						
Pre T_1 or stage I	0.55	2.10	5.04	57.61	1.3862	4.68
Pre T_2 or stage II	3.26	10.2	29.4	62.60	1.3912	6.92
Post T_4 or stage III	2.38	9.40	30.2	47.06	1.4016	8.08[b]
Pure gelatin and CTAB						
0.2 g% gelatin	1.35	6.31	13.7	32.22 (=δ_G)	1.3724	4.05
CTAB (at stage I, pre cmc)	0.45	2.56	5.94	–	–	–
CTAB (at stage III, post cmc)	1.76	13.7	24.0	40.17	1.3902	11.2

[a] Pre T_1, pre T_2 and post T_4 corresponds to 0.013, 0.033 and 3.06 mM CTAB either in pH 9 buffer medium (for pure surfactant) or in 0.2 g% gelatin (for the interacted species).
[b] Γ^T_{max} as calculated using Eq. (1) at T_4 is 0.17 mg m^{-2}[35].

that dried up in air [67,68]. By zooming it on a smaller length scale, the individual structures of the GS^I_n complex (Inset, Fig. 8A) became visible. They appeared as patches in black and white shades due to the difference in the intensity of the reflected beam. While SEM characterized the desolvated surface morphology of a sample, AFM characterized its solvated topography (Fig. 8B, a). The 'interlinked bean shaped domains' had the maximum roughness (Table 2). AFM results produced scattered and merged high profile aggregates of size ~500–650 nm (a significant enhancement in size from 300 nm from that of gelatin aggregates) with a mean height of 10.2 nm. A substantial enhancement in rms roughness of 3.26 nm of the region was observed. It has been found that the bean shaped features have a higher altitude than the average height profile of the projected surface. A cross sectional analysis of the bordered region of Fig. 8B (a), across line 1 (Inset, Fig. 8C) has revealed a typical binodal or trinodal distribution of the beans, when the height (along Z-axis) was plotted against distance (along *X*-axis). The peak width of 170 nm of the middle node was nearly same for all. The peak (considering the highest middle one of a node) to valley distance varied from 8.5–11 nm on an average. Globular structures of aggregates were mostly observed [27]. Nodular forms were rarely found [27,28]. The phase imaging has, however, revealed a distinct morphology of the aggregates (Fig. 8B, b).

Since GS^B_m was essentially a bulk species, the domain feature of the monolayer was exclusively for the surface active GS^I_n. But morphologies of GS^I_n at stages I and II were different. At II, the adsorbed film was rigid and compact due to the entanglements of gelatin chains and a strong cohesion between the hydrophobic entities of protein and amphiphile tail [69]. This enhanced both the surface roughness and the mean height of the profile. Gradual merging of domains caused a slow conversion of GS^I_n to GS^B_m (as evidenced from LB). Such a morphological change at the interface before cac has been rarely documented.

3.4.3.3. Post T_4 or stage III. More CTAB addition led to the collapse of interfacial structures with gradual desolvation of the precipitate (coacervate) and formation of $GS_m(CTAB)_{MS}$ in the bulk following process E or PE [35]. We were interested to elucidate the interfacial topology in the post T_4 region. SEM image has expectedly depicted (Fig. 9A) compact mosaic morphology of solvent-free particles with smaller dimensions. Monomeric surfactants occupy the interface in

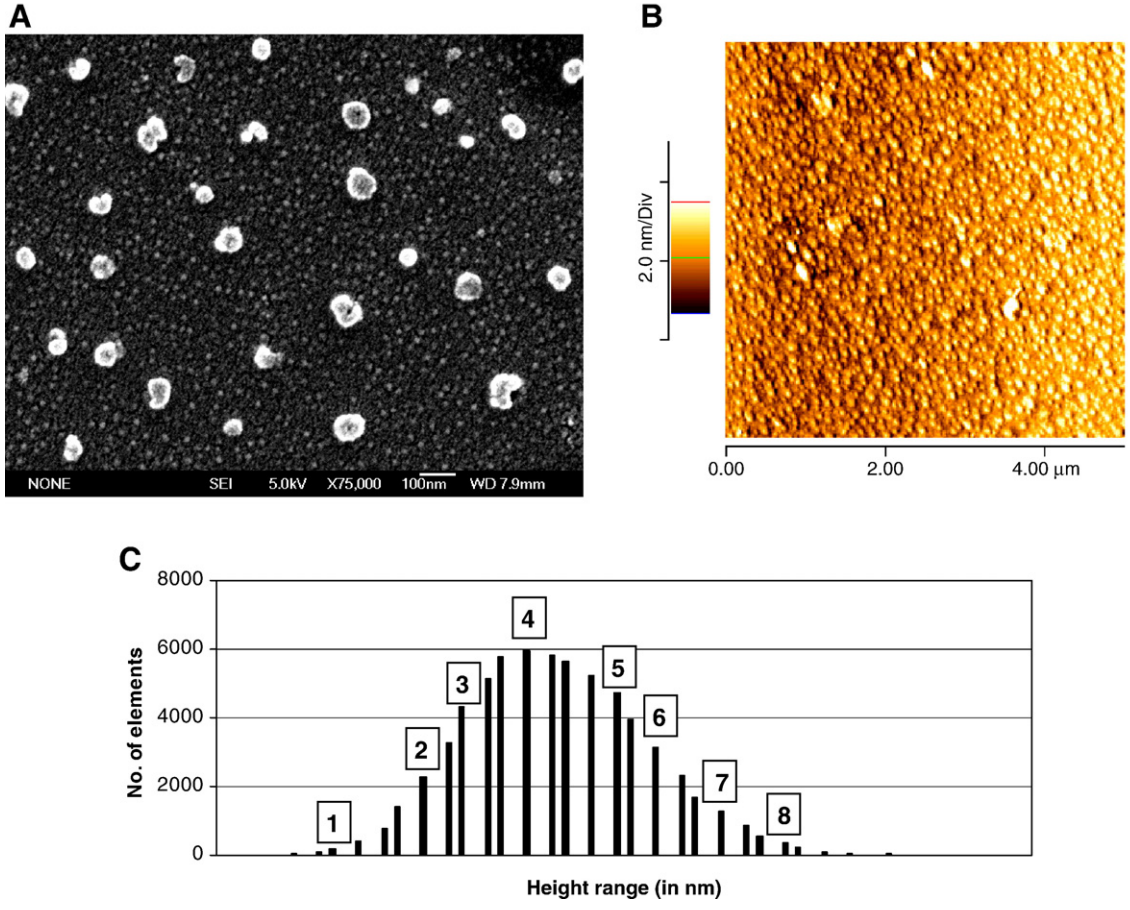

Fig. 7. SEM and AFM images of gelatin–CTAB interaction at [gelatin]=0.2 g% and [CTAB]=0.013 mM (Pre T_1 or stage I). A, SEM images showing presence of high profile protein clusters of reduced dimension. B, Corresponding AFM image of the system. C, Histogram plot of the region in Fig. 7B (Standard deviation=0.6946). The bars are marked from 1–8, corresponding to height ranges (in nm) 1, 0.708–0.787; 2, 1.259–1.338; 3, 1.495–1.574; 4, 1.889–1.967; 5, 2.439–2.518; 6, 2.675–2.754; 7, 3.069–3.148; 8, 3.462–3.541.

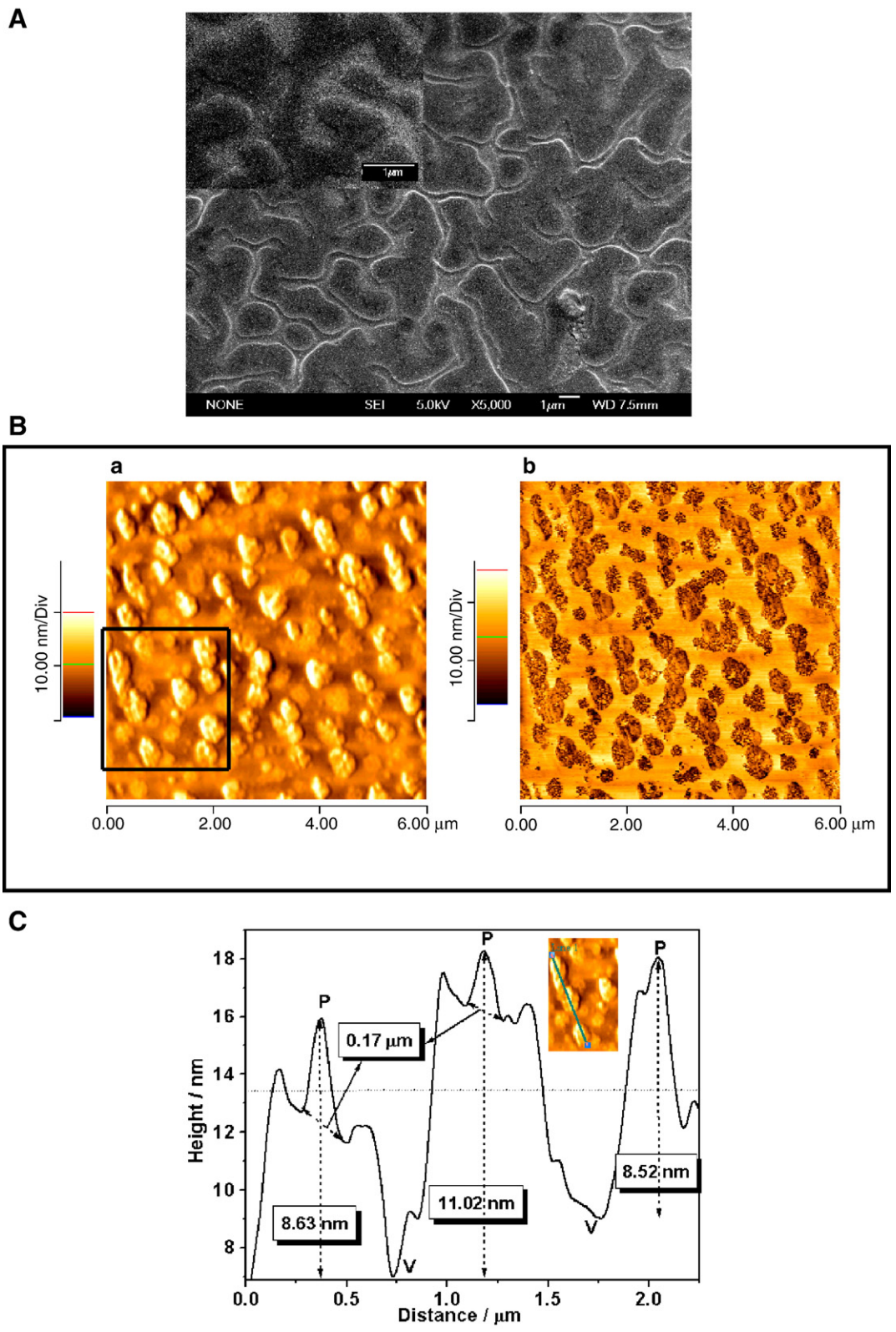

Fig. 8. SEM and AFM images of gelatin–CTAB interaction at [gelatin]=0.2 g% and [CTAB]=0.033 mM (Pre T_2 or stage II). A, SEM image at 5000 magnification. Inset: image at 15,000 magnification. B, Topographic (a) and phase mode (b) AFM images. C, Cross sectional analysis of the image (in the inset) corresponding to line 1 bar. R_{p-v} denotes the peak (P) to valley (V) distance as marked for the trinodal and binodal peaks. Peak widths of the highest node for the two corresponding peaks were found to be the same. Horizontal line across the figure represents the mean height of the line 1 in the inset. Inset: Projection from the indicated box in Fig. 8B (a).

significant proportion (compared to that in Fig. 5A). At concentration close to cmc, existence of microgel [70], nanogel [69] or sandwich-like [71,72] structures have been illustrated in literature. AFM images obtained for pure CTAB film (Fig. 5E), and that of CTAB film in gelatin environment (Fig. 9B) have witnessed both dissimilarity and similarity. The texture (average roughness) lied within 2.38 nm in contrast with 1.76 nm for the pure CTAB film. To some extent it has mimicked the petal-like morphology of pure CTAB film at this concentration

(Fig. 5E), thereby ensuring that the latter was the predominant species at the interface.

A steady increase in $\overline{H}$ or R_{p-v} value in region analysis along the path I→II (Fig. 1) has suggested that the film was condensing with progressive CTAB addition as observed on poly(acrylamide sulfonate)-CTAB combinations by Jain et al.[16]. Large condensation of films for the lower homologues of alkyltrimethylammonium bromide with gelatin made the interface insensitive to minor changes in the tensiometric profile, as reported earlier [35]. The parameters (R_{rms}, $\overline{H}$ and R_{p-v}) decreased from that of pure gelatin on CTAB addition at stage I. These values are tabulated in Table 2. At stage II, roughness and mean height were at the maximum. Post interacting stage III has such values quite close to that of pure CTAB at the said concentration. The presence of CTAB monomers, along with a minor fraction of unreacted G^I or GS^I_n, as proposed earlier was investigated [35].

3.5. Ellipsometric results

The adsorption features of a film, viz., the thickness, refractive index of layers formed and the total amount of adsorbed material at the interface can be ascertained by ellipsometry. The *π–A* isotherms for BSA, lysozyme and β-casein were weakly affected after reaching a threshold [protein], but adsorption increased in layers due to van der Waals or dipole–dipole interaction between the fragments [73]. β-lactoglobulin (being less capable of forming intermolecular bonds) has failed to form a second adsorption layer. Tensiometric or pressure isotherm results have indicated that π increased with [gelatin] (Inset, Fig. 2A). A 0.2 g% protein film formed a thickness of 32.2 nm; earlier report on 0.1% gelatin at pH 6.5 evidenced a thickness of ~40 nm [51]. In the pre T_1 region, the observed thickness of 57.6 nm was greater than the gelatin layer. Adsorption of CTAB on gelatin formed GS^I_n, which produced a thickening effect on the layer. Previous ellipsometric study on DNA-cationic surfactant has evidenced quite thick surface layer due to multilayer adsorption [74]. Both thickness (δ_x), and refractive index (n_x) enhanced with CTAB addition (Table 2). The adsorption or desorption of the spread substance could be judged by evaluating $\Delta\delta$ ($=\delta_x-\delta_G$), where δ_G refers to the thickness of 0.2 g% gelatin [75]. Values of both δ_x and δ_G are presented in Table 2. The results showed fair adsorption of CTAB on gelatin.

Further thickening of the surface film was observed in the pre T_2 (cac) region. A close association of the protein backbone with surfactant tail was accounted for the enhancement in thickness. Surface properties changed drastically when the [surfactant] exceeded cac, but surface layers became more complex as [CTAB] approached cac [76]. Illustrations from SEM and AFM techniques (Fig. 8) revealed change in surface morphology that started well below the cac.

A drastic reduction of ~16 nm in thickness was observed in the post T_4 region. It was slightly greater than 40.2 nm thick pure CTAB film at this concentration. This depletion was similar to the NaPSS/DTAB system, in which depletion initiated beyond the second cmc, with a complete dissolution at a concentration ~200 times cmc [70]. Here three simultaneous processes were involved: 1) a gradual dissolution of large aggregates of surface inactive GS^C_m, 2) appearance of a pure surfactant monolayer which was more surface active; and 3) a scanty presence of interfacially adsorbed GS^I_n or unreacted G^I. Their combined effect produced a penultimate thickness of 47.1 nm at T_4. In contrary, Taylor et al. [71] have reported a thick (60–100 Å) sandwich like close packed monolayer at concentrations closer to cmc. The presence of water might have a reducing effect [74]. Interfacial thickness could approach to that of a pure monolayer on further surfactant addition, if the contribution of GS^I_n or G^I was neglected. In our previous study [35], we have observed a disparity between γ_{cmc} and γ_{T_4}; thus, the interfacial texture of a pure monolayer film at the air/buffer interface was physicochemically different from a polyelectrolyte influenced surfactant film. Earlier report on gelatin–SDBS system has documented a thickness of ~40–45 nm in the post cmc region [51]. Surface excess (Γ^E_{max}) estimated from Eq. (2), increased with CTAB addition (Table 2). But the surface excess of pure CTAB at the concentration of stage III exceeded that of protein–CTAB complex at the said concentration. The presence of less surface active species like GS^I_n and G^I than CTAB was accountable for this observation. At T_4, Γ^T_{max} obtained from Gibbs adsorption Eq. (1) was 0.17 mg m^{-2}, which was nearly 50 times less than that obtained from Eq. (2) at post T_4. Local concentration of protein-surfactant complex offered non significant change in π, which remained undetected by tensiometry [39].

Ellipsometric results have evidenced enhancement of thickness of the interfacial layer: multilayer formation was envisaged. Multilayer formation at varied (bio)polymer/amphiphile mole ratios has been documented in literature. The neutron [71,72,77,78] and X-ray reflectivity [79], and dilational rheological studies [80] have shown increased adsorption layer thickness for relatively concentrated solutions of sodium polystyrenesulfonate (NaPSS)-ATAB, poly(vinylpyridinium chloride) (PVPCl)-SDS in presence of NaCl, branched polyethyleneamine (PEI)-SDS and sodium polyacrylate (NaPA)-DTAB at high pH, and in 7 wt.% gelatin-SDS. In our previous study [35], on interaction of gelatin with DTAB (C_{12}) and TTAB (C_{14}), a flattened

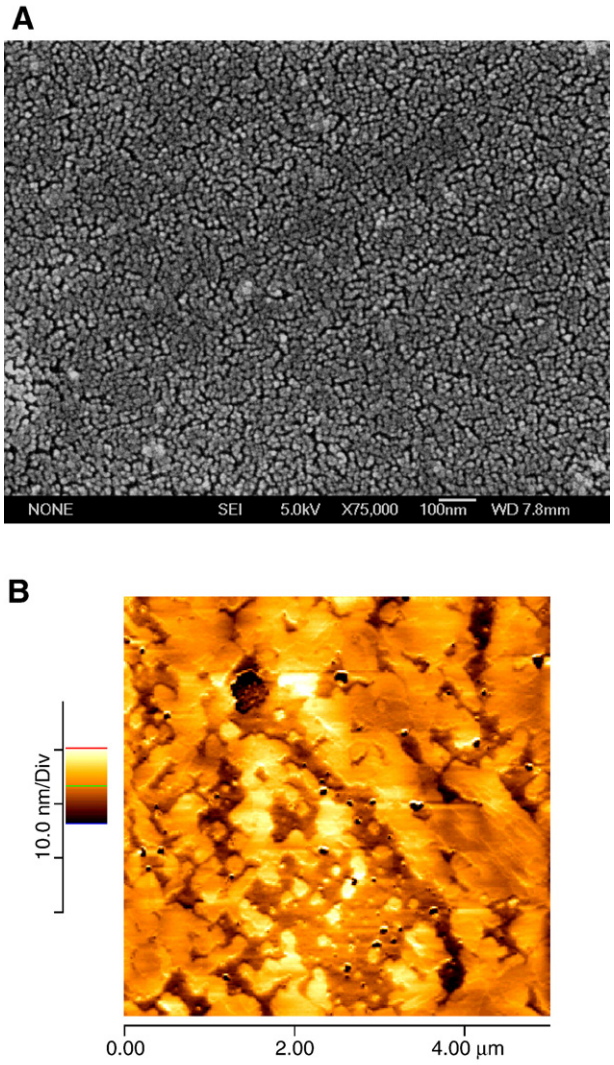

Fig. 9. SEM and AFM images of gelatin–CTAB interaction at [gelatin]=0.2 g% and [CTAB]=3.06 mM (Post T_4 or stage III). A, SEM image of the system. B, AFM image of the system.

tensiometric profile in the lower concentration was observed. Similar profiles were also evidenced in PVPCl-SDS-NaCl [77], TTAB-PDMDAAC/0.1 M NaCl [81], PEI-SDS [78] and in 7 wt.% gelatin–SDS system [80]. These experimental methods supported multilayered structure formation beyond certain surface concentration. For surface-active polyelectrolyte like gelatin, this saturation started at a lower concentration state, whereas surface inactive NaPSS formed subsurface-layered micelles or bilayers wrapped polymer chain at higher concentration state [70]. Ellipsometry also has shown surface gelation at a low surfactant concentration before bulk PSS-ATAB complex precipitation, and during resolubilization of the complex at higher surfactant concentration [82,83]. From the study of the adsorption kinetics of multilayered interfacial PDMDAAC-SDS complex, it has been found that surface tension remained constant throughout the range, whereas the thickness increased as found from ellipsometry [39].

4. Conclusive comprehension

Interfacial behavior of pure gelatin and CTAB at pH 9 and subphase ionic strength of 0.005 was studied separately and in combination at varied compositions. The gelatin–CTAB interacted interfacial products selected for morphological and structural study were at stages I, II and III with reference to Fig. 1. They corresponded to the interfacial layers for the formation of GS^{I}_{n} at pre T_1, its transformed state GS^{B}_{m} at pre T_2, and the state of gelatin–CTAB aggregate embedded micelle at T_4, respectively. π of pure gelatin spread on the aqueous buffer surface at different concentrations increased with time in two stages to reach equilibrium; the propensity of protein anchoring on the water surface became time dependent. The hydrophobic–hydrophilic balance at the interface got adjusted with time to produce an equilibrium π value that was directly proportional to [gelatin] and time. The monolayer was poorly compressible, like typical condensed films with low collapse pressures. The area per molecule varied from 69 to 0.001 nm^2 $molecule^{-1}$ in the [gelatin] ranging between 5 μg to 0.2 g%. Kinetics of the interaction profile between gelatin and CTAB at the interface has revealed that T_1–T_2 regime acted as a pre transition stage for the process B. Distinct structural features of gelatin–CTAB aggregates at the interface arose prior to the formation of cac. Gradual merging of domains has paved the way for the transformation that has exhibited a reduction in the maximum π along with a fall in the limiting area per molecule.

The surface film morphological study from SEM, AFM and ellipsometry has further supported the above mentioned states. On addition of CTAB (stage I), the surface became smoother, typically like that of a CTAB monolayer at the said concentration limit with a much reduced dimension of the clusters (as observed for pure gelatin). The surface topology was in the midway between pure gelatin and pure CTAB films. This change has been attributed to the initiation of GS^{I}_{n} formation via electrostatic interaction between negatively charged gelatin and CTA^{+}. Further addition resulted in a condensed bean shaped domain formation, which was the ultimate topography of surface active GS^{I}_{n}, an electrostatically and hydrophobically interacted gelatin–CTAB combination (at stage II). The stage acted as a pre transition state for partitioning of GS^{I}_{n} to GS^{B}_{m} via process B. Surface parameters like, roughness, thickness and mean height of the film were at their maxima at this stage, with a moderate refractive index. The stage III marking the end of the interaction profile revealed a complex topography with the surface having a significant contribution from CTAB monomers. Refractive index of the LB film was at its maximum at the post interaction stage III. The presence of other species like unchanged GS^{I}_{n} and/or unreacted G^{I} made all surface parameters different from that of a pure monolayer film. Analysis of behaviors of surface films of gelatin and gelatin–CTAB combinations in terms of a suitable model requires further studies under controlled experimental conditions.

Acknowledgements

D. M. thanks the Council of Scientific and Industrial Research, Govt. of India for financial support. S. P. M. thanks the Jadavpur University for an Emeritus Professorship and the Indian National Science Academy for an Honorary Scientist position. We thank the director, CGCRI, Kolkata, for permitting us to use their ellipsometric facility. We also thank Mr. R. Banik and Mr. S. Majhi, IACS, Kolkata, for AFM and SEM measurements, respectively.

References

[1] V.B. Fainerman, E.H. Lucassen-Reynders, R. Miller, Description of the adsorption behaviour of proteins at water/fluid interfaces in the framework of a two-dimensional solution model, Adv. Colloid Interface Sci. 106 (2003) 237–259.
[2] J.B. Peng, G.T. Barnes, I.R. Gentle, The structures of Langmuir–Blodgett films of fatty acids and their salts, Adv. Colloid Interface Sci. 91 (2001) 163–219.
[3] P. Dynarowicz-Latka, A. Dhanabalan, O.N. Oliveira Jr, Modern physicochemical research on Langmuir monolayers, Adv. Colloid Interface Sci. 91 (2001) 221–293.
[4] Y-S. Seo, F. Ahmad, K. Shin, J-M. Song, J-S. Kim, M.H. Rafailovich, J. Sokolov, S.K. Satija, Interfacial behavior of randomly charged sulfonated polystyrene (PSS) at the air/water interface, Colloids Surf. A 313–314 (2008) 660–665.
[5] L. Goracci, R. Germani, J.F. Rathman, G. Savelli, Anomalous behavior of amine oxide surfactants at the air/water interface, Langmuir 23 (2007) 10525–10532.
[6] R.S.G. Krishnan, S. Thennarasu, A.B. Mandal, Self-assembling characteristics of a new nonionic gemini surfactant, J. Phys. Chem. B. 108 (2004) 8806–8816.
[7] T. Zhang, P.R. Dvornic, S.N. Kaganove, A comparative study of amphiphilic pamam dendrimers at the air/water interface with different hydrophobe attachment groups, Langmuir 23 (2007) 10589–10597.
[8] M.A. Alsina, C. Mestres, F. Rabanal, M.A. Busquets, F. Reig, Miscibility of HBV peptides and dipalmitoylphosphatidylcholine in monolayers, Langmuir 9 (1993) 1129–1133.
[9] S. Mukherjee, K. Maiti, M. Fritzen-Garcia, S.C. Bhattacharya, K. Nag, A.K. Panda, S.P. Moulik, Physicochemical studies on goat pulmonary surfactant, Biophys. Chem. 134 (2008) 1–9.
[10] H. Nakahara, S. Nakamura, T. Hiranita, H. Kawasaki, S. Lee, G. Sugihara, O. Shibata, Mode of interaction of amphiphilic-helical peptide with phosphatidylcholines at the air/water interface, Langmuir 22 (2006) 1182–1192.
[11] D.H. McCullough, R. Grygorash, S.L. Regen, Fluorocarbon crowning: Langmuir–Blodgett deposition versus self-assembly at molecularly rough surfaces, Langmuir 23 (2007) 9606–9610.
[12] E.D. Goddard, R.B. Hannan, Cationic polymer/anionic surfactant interactions, J. Colloid Interface Sci. 55 (1976) 73–79.
[13] T. Kamilya, P. Pal, G.B. Talapatra, Incorporation of ovalbumin within cationic octadecylamine monolayer and a comparative study with zwitterionic DPPC and anionic stearic acid monolayer, J. Colloid Interface Sci. 315 (2007) 464–474.
[14] P. Stroeve, M.J. Hwa, Effects of pH on gegenion complex Langmuir–Blodgett films, Thin Solid Films 284–285 (1996) 561–563.
[15] N.J. Jain, P.-A. Albouy, D. Langevin, Study of adsorbed monolayers of a cationic surfactant and an anionic polyelectrolyte at the air/water interface. Role of the polymer charge density, Langmuir 19 (2003) 8371–8379.
[16] N.J. Jain, P.-A. Albouy, D. Langevin, Study of adsorbed monolayers of a cationic surfactant and an anionic polyelectrolyte at the air/water interface, Langmuir 19 (2003) 5680–5690.
[17] W. Meier, J.J. Ramsden, Surface pressure determines the interaction between poly (oxyethylene) and a surfactant bilayer, J. Phys. Chem. 100 (1996) 1435–1438.
[18] Y. Matsumoto, H. Nakahara, Y. Moroi, O. Shibata, Langmuir monolayer properties of perfluorinated double long-chain salts with divalent counterions of separate electric charge at the air/water interface, Langmuir 23 (2007) 9629–9640;
K. Hoda, H. Nakahara, S. Nakamura, S. Nagadome, G. Sugihara, N. Yoshino, O. Shibata, Langmuir monolayer properties of the fluorinated-hydrogenated hybrid amphiphiles with dipalmitoylphosphatidylcholine (DPPC), Colloids Surf. B 47 (2006) 165–175.
[19] G. Zavala, Atomic force microscopy, a tool for characterization, synthesis and chemical processes, Colloid Polym. Sci. 286 (2008) 85–95.
[20] A. Svensson, J. Sjöström, T. Scheel, L. Piculell, Phases and structures of a polyion–surfactant ion complex salt in aqueous mixtures: cationic hydroxyethyl cellulose with dodecylsulfate counterions, Colloids Surf. A 228 (2003) 91–106.
[21] E. Staples, I. Tucker, J. Penfold, N. Warren, R.K. Thomas, D.J.F. Taylor, Organization of polymer–surfactant mixtures at the air/water interface: sodium dodecylsulfate and poly(dimethyldiallylammonium chloride), Langmuir 18 (2002) 5147–5153.
[22] Y. Li, J. Xia, P.L. Dubin, Complex formation between polyelectrolyte and oppositely charged mixed micelles: static and dynamic light scattering study of the effect of polyelectrolyte molecular weight and concentration, Macromolecules 27 (1994) 7049–7055.
[23] S. Nagadome, N.S. Suzuki, Y. Mine, T. Yamaguchi, H. Nakahara, O. Shibata, C-H. Chang, G. Sugihara, Monolayers (Langmuir films) behavior of multi-component systems composed of a bile acid with different sterols and with their 1:1 mixtures, Colloids Surf. B 58 (2007) 121–136.
[24] M. Radmacher, M. Fritz, J.P. Cleveland, D.A. Walters, P.K. Hansma, Imaging adhesion forces and elasticity of lysozyme adsorbed on mica with the atomic force microscope, Langmuir 10 (1994) 3809–3814;

D.T. Kim, H.W. Blanch, C.J. Radke, Direct imaging of lysozyme adsorption onto mica by atomic force microscopy, Langmuir 18 (2002) 5841–5850.
[25] V. Subramanian, W.A. Ducker, Counterion effects on adsorbed micellar shape: experimental study of the role of polarizability and charge, Langmuir 16 (2000) 4447–4454.
[26] G. Binnig, C.F. Quate, C. Gerber, Atomic force microscope, Phys. Rev. Lett. 56 (1986) 930–933;
D. Pastre, L. Hamon, F. Landousy, I. Sorel, M.-O. David, A. Zozime, E. Le Cam, O. Pietrement, Anionic polyelectrolyte adsorption on mica mediated by multivalent cations: a solution to DNA imaging by atomic force microscopy under high ionic strengths, Langmuir 22 (2006) 6651–6660;
S.E. Fritz, S.M. Martin, C.D. Frisbie, M.D. Ward, M.F. Toney, Structural characterization of a pentacene monolayer on an amorphous SiO_2 substrate with grazing incidence X-ray diffraction, J. Am. Chem. Soc. 126 (2004) 4084–4085;
V.N. Bliznyuk, Y.S. Lipatov, N. Ozdemir, T.T. Todosijchuk, V.N. Chornaya, S. Singamaneni, Atomic force and ultrasonic force microscopy investigation of adsorbed layers formed by two incompatible polymers: polystyrene and poly (butyl methacrylate), Langmuir 23 (2007) 12973–12983.
[27] K.L. Marchin, C.L. Berrie, Conformational changes in the plasma protein fibrinogen upon adsorption to graphite and mica investigated by atomic force microscopy, Langmuir 19 (2003) 9883–9888.
[28] P. Cacciafesta, A.D.L. Humphris, K.D. Jandt, M.J. Miles, Human plasma fibrinogen adsorption on ultraflat titanium oxide surfaces studied with atomic force microscopy, Langmuir 16 (2000) 8167–8175.
[29] L. Chaal, F. Pillier, B. Saidani, S. Joiret, A. Pailleret, C. Deslouis, L. Chaal, F. Pillier, B. Saidani, S. Joiret, A. Pailleret, C. Deslouis, Characterization of counterion and surface influence on micelle formation using tapping mode atomic force microscopy in air, J. Phys. Chem. B. 110 (2006) 21710–21718.
[30] P.G. Mussone, A.W.F. Ip, S.L.M. Schroeder, B.S. Murray, A.F. Miller, Irreversible collapse of poly(vinyl stearate) monolayers at the air/water interface, Langmuir 23 (2007) 3766–3773.
[31] M. Kawaguchi, Thermodynamic, structural and rheological properties of polymer films at the air/water interface, Prog. Polym. Sci. 18 (1993) 341–376.
[32] B.A. Noskov, A.V. Akentiev, D.O. Grigoriev, G. Loglio, R. Miller, Ellipsometric study of nonionic polymer solutions, J. Colloid Interface Sci. 282 (2005) 38–45.
[33] N.C. de Souza, W. Caetano, R. Itri, C.A. Rodrigues, O.N. Oliveira Jr., J.A. Giacometti, M. Ferreira, Interaction of small amounts of bovine serum albumin with phospholipid monolayers investigated by surface pressure and atomic force microscopy, J. Colloid Interface Sci. 297 (2006) 546–553.
[34] P. Wydro, B. Krajewska, K. Hac-Wydro, Chitosan as a lipid binder: a Langmuir monolayer study of chitosan–lipid interactions, Biomacromolecules 8 (2007) 2611–2617.
[35] D. Mitra, S.C. Bhattacharya, S.P. Moulik, Physicochemical studies on the interaction of gelatin with cationic surfactants alkyltrimethylammonium bromides (ATABs) with special focus on the behavior of the hexadecyl homologue, J. Phys. Chem. B. 112 (2008) 6609–6619.
[36] A. Chatterjee, S.P. Moulik, P.R. Majhi, S.K. Sanyal, Studies on surfactant–biopolymer interaction. I. Microcalorimetric investigation on the interaction of cetyltrimethylammonium bromide (CTAB) and sodium dodecylsulfate (SDS) with gelatin (Gn), lysozyme (Lz) and deoxyribonucleic acid (DNA), Biophys. Chem. 98 (2002) 313–327.
[37] S. Maulik, P. Dutta, D.K. Chattoraj, S.P. Moulik, Biopolymer–surfactant interactions: 5: Equilibrium studies on the binding of cetyltrimethylammonium bromide and sodium dodecylsulfate with bovine serum albumin, β-lactoglobulin, hemoglobin, gelatin, lysozyme and deoxyribonucleic acid, Colloids Surf. B 11 (1998) 1–8.
[38] E.D. Goddard, Polymer–surfactant interaction part II. Polymer and surfactant of opposite charge, Colloids Surf. 19 (1986) 301–329.
[39] B.A. Noskov, D.O. Grigoriev, S.-Y. Lin, G. Loglio, R. Miller, Dynamic surface properties of polyelectrolyte/surfactant adsorption films at the air/water interface: poly(diallyldimethylammonium chloride) and sodium dodecylsulfate, Langmuir 23 (2007) 9641–9651.
[40] W.R. Birch, M.A. Knewtson, S. Garoff, R.M. Suter, S. Satija, The molecular structure of autophobed monolayers and precursing films of a cationic surfactant on the silicon oxide/silicon surface, Colloids Surf. A 89 (1994) 145–155.
[41] P. Tippmann-Krayer, R.M. Kenn, H. Mohwald, Thickness and temperature dependent structure of Cd arachidate Langmuir–Blodgett films, Thin Solid Films 210–211 (1992) 577–582 Part 2.
[42] A. Malik, M.K. Durbin, A.G. Richter, K.G. Huang, P. Dutta, Structures of head-group and tail-group monolayers in a Langmuir–Blodgett film, Phys. Rev. B 52 (1995) R11654–R11657.
[43] D. Blaudez, T. Buffeteau, N. Castaings, B. Desbat, J.M. Turlet, Organization in pure and alternate deuterated cadmium arachidate monolayers on solid substrates and at the air/water interface studied by conventional and differential Fourier transform infrared spectroscopies, J. Chem. Phys. 104 (1996) 9983–9993.
[44] A. Ulaman, An Introduction to Ultrathin Organic Films from Langmuir–Blodgett to Self-assembly, Academic Press, New York, 1991.
[45] K. Kim, C. Kim, Y. Byun, Preparation of a dipalmitoylphosphatidylcholine/cholesterol Langmuir–Blodgett monolayer that suppresses protein adsorption, Langmuir 17 (2001) 5066–5070.
[46] M. Landgren, B. Joensson, Determination of the optical properties of silicon/silica surfaces by means of ellipsometry, using different ambient media, J. Phys. Chem. 97 (1993) 1656–1660.
[47] M. Fritz, M. Radmacher, J.P. Cleveland, M.W. Allersma, R.J. Stewart, R. Gieselmann, P. Janmey, C.F. Schmidt, P.K. Hansma, Imaging globular and filamentous proteins in physiological buffer solutions with tapping mode atomic force microscopy, Langmuir 11 (1995) 3529–3535.
[48] K. Vallieres, P. Chevallier, C. Sarra-Bournet, S. Turgeon, G. Laroche, AFM imaging of immobilized fibronectin: does the surface conjugation scheme affect the protein orientation/conformation? Langmuir 23 (2007) 9745–9751.
[49] J.A. de Feijter, J. Benjamins, F.A. Veerde, Ellipsometry as a tool to study the adsorption behavior of synthetic and biopolymers at the air/water interface, Biopolymers 17 (1978) 1759–1772.
[50] M. Kawaguchi, A. Takahashi, Polymer adsorption at solid–liquid interfaces, Adv. Colloid Interface Sci. 37 (1992) 219–317.
[51] D. Muller, M. Malmsten, B. Bergenstahl, J. Hessing, J. Olijve, F. Mori, Competitive adsorption of gelatin and sodium dodecylbenzenesulfonate at hydrophobic surfaces, Langmuir 14 (1998) 3107–3114.
[52] M. Cárdenas, T. Nylander, B. Lindman, DNA and cationic surfactants at solid surfaces, Colloids Surf. A 270–271 (2005) 33–43.
[53] H. Motschmann, R. Teppner, in: D. Mobius, R. Miller (Eds.), Novel Methods to Study Interfacial Layers (Studies in Interface Science), vol. 11, Elsevier, Amsterdam, 2001, p. 1.
[54] R.A. Campbell, P.A. Ash, C.D. Bain, Dynamics of adsorption of an oppositely charged polymer–surfactant mixture at the air/water interface: poly(dimethyldiallylammonium chloride) and sodium dodecylsulfate, Langmuir 23 (2007) 3242–3253.
[55] S. Xu, S. Damodaran, The role of chemical potential in the adsorption of lysozyme at the air/water interface, Langmuir 8 (1992) 2021–2027.
[56] S. Sundaram, J.K. Ferri, D. Vollhardt, K.J. Stebe, Surface phase behavior and surface tension evolution for lysozyme adsorption onto clean interfaces and into DPPC monolayers: Theory and experiment, Langmuir 14 (1998) 1208–1218.
[57] G.L.J. Gaines, Insoluble Monolayer at Liquid/Air Interfaces, Wiley, New York, 1966.
[58] M. Kawaguchi, W. Saito, T. Kato, Poly(N-isopropylacrylamide) films at the air/water interface, Macromolecules 27 (1994) 5882–5884.
[59] A. Dhanabalan, L. Gaffo, A.M. Barros, W.C. Moreira, O.N. Oliveira Jr., Surface pressure and surface potential isotherms of ytterbium bisphthalocyanine Langmuir monolayers, Langmuir 15 (1999) 3944–3949.
[60] H. Wang, W. Li, H. Ding, Y. Zhang, S. Xi, A method to identify the collapse of monolayers at the air/water interface, Thin Solid Films 284–285 (1996) 119–121.
[61] (a) N.R. Pallas, B.A. Pethica, Liquid-expanded to liquid-condensed transition in lipid monolayers at the air/water interface, Langmuir 1 (1985) 509–513;
(b) V.B. Fainerman, S.A. Zholob, M.E. Leser, M. Michel, R. Miller, Adsorption from mixed ionic surfactant/protein solutions: analysis of ion binding, J. Phys. Chem. B 108 (2004) 16780–16785.
[62] R.K. Iler, The Chemistry of Silica, John Wiley and Sons, New York, 1979, p. 680.
[63] T. Gu, Z. Huang, Thermodynamics of hemimicellization of cetyltrimethylammonium bromide at the silica gel/water interface, G. L. J. 40 (1989) 71–76.
[64] S. Manne, J.P. Cleveland, H.E. Gaub, G.D. Stucky, P.K. Hansma, Direct visualization of surfactant hemimicelles by force microscopy of the electrical double layer, Langmuir 10 (1994) 4409–4413.
[65] Y. Seo, C.Y. Cho, M. Hwangbo, H.J. Choi, S.M. Hong, Effect of temperature on the interfacial behavior of a polystyrene-b-poly(methyl methacrylate) diblock copolymer at the air/water interface, Langmuir 24 (2008) 2381–2386.
[66] J.G. Forbes, A.J. Jin, K. Wang, Atomic force microscope study of the effect of the immobilization substrate on the structure and force-extension curves of a multimeric protein, Langmuir 17 (2001) 3067–3075.
[67] J.H. Buckingham, J. Lucassen, F. Hollway, Surface properties of mixed solutions of poly-L-lysine and sodium dodecylsulfate: I. equilibrium surface properties, J. Colloid Interface Sci. 67 (1978) 423–431.
[68] A. Asnacios, D. Langevin, J.-F. Argillier, Complexation of cationic surfactant and anionic polymer at the air/water interface, Macromolecules 29 (1996) 7412–7417.
[69] B.A. Noskov, G. Loglio, R. Miller, Dilational viscoelasticity of polyelectolyte/surfactant adsorption films at the air/water interface: dodecyltrimethylammonium bromide and sodium poly(styrenesulfonate), J. Phys. Chem. B 108 (2004) 18615–18622.
[70] C. Monteux, C.E. Williams, J. Meunier, O. Anthony, V. Bergeron, Adsorption of oppositely charged polyelectrolyte/surfactant complexes at the air/water interface: formation of interfacial gels, Langmuir 20 (2004) 57–63.
[71] D.J.F. Taylor, R.K. Thomas, P.X. Li, J. Penfold, Adsorption of oppositely charged polyelectrolyte/surfactant mixtures. neutron reflection from alkyltrimethylammonium bromides and sodium poly(styrenesulfonate) at the air/water interface: the effect of surfactant chain length, Langmuir 19 (2003) 3712–3719.
[72] D.J.F. Taylor, R.K. Thomas, J. Penfold, The adsorption of oppositely charged polyelectrolyte/surfactant mixtures: neutron reflection from dodecyltrimethylammonium bromide and sodium poly(styrene sulfonate) at the air/water interface, Langmuir 18 (2002) 4748–4757.
[73] D.O. Grigoriev, V.B. Fainerman, A.V. Makievski, J. Krägel, R. Wüstneck, R. Miller, β-Casein bilayer adsorption at the solution/air interface: experimental evidences and theoretical description, J. Colloid Interface Sci. 253 (2002) 257–264.
[74] D. McLoughlin, D. Langevin, Surface complexation of DNA with a cationic surfactant, Colloids Surf. A 79 (2004) 79–87 and references therein.
[75] A. Asnacios, D. Langevin, J.F. Argillier, Mixed monolayers of cationic surfactants and anionic polymers at the air/water interface: surface and ellipsometry studies, Eur. Phys. J. B 5 (1998) 905–911.
[76] H. Ritacco, D. Kurlat, D.J. Langevin, Properties of aqueous solutions of polyelectrolytes and surfactants of opposite charge: surface tension, surface rheology, and electrical birefringence studies, J. Phys. Chem. B 107 (2003) 9146–9158.
[77] D.J.F. Taylor, R.K. Thomas, J.D. Hines, K. Humphreys, J. Penfold, The adsorption of oppositely charged polyelectrolyte/surfactant mixtures at the air/water interface: neutron reflection from dodecyltrimethylammoniumbromide/sodium poly(styrenesulfonate) and sodium dodecylsulfate/poly(vinyl pyridinium chloride), Langmuir 18 (2002) 9783–9791.
[78] J. Penfold, I. Tucker, R.K. Thomas, J. Zhang, Adsorption of polyelectrolyte/surfactant mixtures at the air/solution interface: poly(ethyleneimine)/sodium dodecylsulfate, Langmuir 21 (2005) 10061–10073.

[79] D. Vaknin, S. Dahlke, A. Travesset, G. Nizri, S. Magdassi, Induced crystallization of polyelectrolyte–surfactant complexes at the gas–water interface, Phys. Rev. Lett. 93 (2004) 218302-1–218302-4.
[80] A. Rao, J. Kim, R.K. Thomas, Interfacial rheological studies of gelatin–sodium dodecylsulfate complexes adsorbed at the air/water interface, Langmuir 21 (2005) 617–621.
[81] J. Penfold, I. Tucker, R.K. Thomas, D.J.F. Taylor, X.L. Zhang, C. Bell, C. Breward, P. Howell, The interaction between sodium alkyl sulfate surfactants and the oppositely charged polyelectrolyte, polyDMDAAC, at the air/water interface: the role of alkyl chain length and electrolyte and comparison with theoretical predictions, Langmuir 23 (2007) 3128–3136.
[82] C. Monteux, C.E. Williams, V. Bergeron, Interfacial microgels formed by oppositely charged polyelectrolytes and surfactants. Part 2. Influence of surfactant chain length and surfactant/polymer ratio, Langmuir 20 (2004) 5367–5374.
[83] C. Monteux, M.-F. Llauro, D. Baigl, C.E. Williams, O. Anthony, V. Bergeron, Interfacial microgels formed by oppositely charged polyelectrolytes and surfactants. 1. influence of polyelectrolyte molecular weight, Langmuir 20 (2004) 5358–5366.